Nanomechanical Properties of Arachidic Acid Langmuir−Blodgett Films

Gerard Oncins,[†,‡,§] Joan Torrent-Burgués,[#] and Fausto Sanz*[,†,‡,§]

CIBER-BBN, Department of Physical Chemistry, Universitat de Barcelona and Bioengineering Institute of Catalonia, Martí i Franquès 1, 08028 Barcelona, Spain, and Department of Chemical Engineering, Universitat Politècnica de Catalunya, Colom 1, 08222 Terrassa (Barcelona), Spain

Received: July 16, 2007; In Final Form: November 15, 2007

The nanomechanical properties of Langmuir−Blodgett monolayers of arachidic acid extracted at surface pressures of 1, 15, and 35 mN/m and deposited on mica were investigated by atomic force microscopy, force spectroscopy, and lateral force microscopy. It was experimentally demonstrated that the arachidic acid molecular orientation depends on the extraction pressure. According to this, tilting angles of 50, 34, and 22° with respect to the surface perpendicular were detected and identified as conformations that maximize van der Waals interactions between the arachidic acid alkyl chains. The vertical force needed to puncture the monolayers with the AFM tip strongly depends on the molecular tilting angles attained at different monolayer extraction surface pressures, obtaining values that range from 13.07 ± 3.24 nN for 50° to 22.94 ± 5.49 nN for 22° tilting angles. The different molecular interactions involved in the monolayer cohesion are discussed and quantitatively related to the experimental monolayer breakthrough forces. The friction measurements performed from low vertical forces up to monolayer disruption reveal the existence of three well-defined regimes: first, a low friction response due to the elastic deformation of the monolayer, which is followed by a sharp increase in the friction force due to the onset of a sudden plastic deformation. The last regime corresponds to the monolayer rupture and the contact between tip and substrate. The friction coefficient of the substrate is seen to depend on the monolayer extraction pressure, a fact that is discussed in terms of the relationship between the sample compactness and its rupture mechanism.

Introduction

Since its development in 1935,[1] the Langmuir−Blodgett technique (LB) has been widely used to prepare all kinds of ordered structures as varied as phospholipid bilayers[2] or nanowire arrays.[3] The possibility to control the surface pressure (Π) and consequently the area per molecule (or particle) during the transfer to a solid substrate makes this technique a powerful way to prepare surfaces with tailored chemical, structural, and mechanical properties. This fact, besides the emergence of micro- and nanoelectromechanical systems (MEMS and NEMS) and the consequent necessity of producing lubricants at a molecular level, have led to an extensive use of LB films, not only to obtain viable low-friction coatings for the electronics industry[4,5] but also to use them as models to study molecular interactions and interfacial phenomena. Regarding these applications, fatty acid LB films have become useful systems because of their linear geometry, amphiphilic nature, and high mechanical stability and durability.

Down to the micro- and nanometric ranges, fatty acid mono- and bilayers have been studied by atomic force microscopy (AFM) and related techniques such as lateral force microscopy (LFM), which was applied in the past to a variety of films on surfaces[6−11] including lipid bilayers and membranes,[12,13] especially highlighting the chemical, compositional, and structural contrast that can be attained by means of these techniques.

Concerning the molecular structure of fatty acid LB films, the cadmium arachidate (CdAr) pattern was resolved using diffraction techniques,[14] obtaining a hexagonal molecular packing where the alkyl chains are perpendicular to the substrate, and later IR measurements concluded that the alkyl chains are in an all-trans conformation.[15] Interestingly, a subsequent AFM molecular resolution study conducted by Mori and Imae[16] confirmed that arachidic acid (AA) LB films extracted at a Π value of 25 mN/m also pack in a hexagonal lattice with molecules perpendicular to the substrate, a fact that was discussed by Evenson et al.,[17] who concluded that the alkyl chain tilt angle depends on the Π value as well as on the area per molecule. In this direction, Kajiyama et al.[18] experimentally demonstrated the concordance between the calculated area per molecule before and after transferring lignoceric (LA) and stearic acid (SA) monolayers to the surface of a mica sheet. Nevertheless, X-ray studies performed on behenic acid (BA) LB films suggested that the monolayer structure was independent of the phase from which deposition took place,[19] and Chunbo et al.[20] reported that 1,2-dipalmitoyl-*sn*-glycero-3-phosphate mono- and trilayers relax to match the mica atomic structure. Moreover, another experimental work concluded that the nanomechanical properties of AA, BA, and SA strongly depend on the Π value,[21] highlighting the key role of the molecular structure and intermolecular interactions in the properties of the transferred films.

The dependence between monolayer thickness and applied vertical force (F_v) was studied by AFM for several fatty acids using both contact and tapping modes, showing that there is an initial monolayer thickness decrease attributed to the creation of gauche defects in the alkyl chain terminal ends at low F_v

* Corresponding author. E-mail: fsanz@ub.edu.
† CIBER-BBN.
‡ Department of Physical Chemistry, Universitat de Barcelona.
§ Bioengineering Institute of Catalonia (IBEC).
# Universitat Politècnica de Catalunya.

10.1021/jp0755544 CCC: $40.75
Published on Web 01/23/2008

values, followed by a constant thickness regime and by a final monolayer rupture after a threshold F_v value is reached.[21] A similar study performed on BA[22] pointed out that the monolayer thickness evolution versus F_v also depends on the monolayer phase, which can be controlled both by changing the temperature or by changing the Π value. According to this, different monolayer phases present different friction force (F_f) versus F_v trends, a fact that highlights the high sensitivity of the F_f signal with respect to the monolayer molecular ordering. Then, solid BA monolayers behave elastically at low F_v values and deform plastically as F_v increases, while fluid BA shows a plasticity independently of the applied F_v.[23]

Although the presence of defects plays a crucial role in the tribological performance of fatty acid monolayers,[24] the composition of the Langmuir film subphase (prior to deposition on a solid substrate) is also important; carboxylic acid groups create H-bonding networks at acidic pH,[16] contributing to a better molecular packing. As the pH value increases, the monolayer stability can also be improved by adding cations that bind electrostatically to the deprotonated carboxyl groups, as was experimentally demonstrated by studying the sample relaxation time and consequent formation of the 3-D structures that appear after monolayer collapse due to the sample compression above the equilibrium surface pressure.[25] Another important factor that shapes the mechanical properties of fatty acid LB monolayers is the length of the alkyl chains, mainly due to the intermolecular van der Waals interactions arising between methylene groups. Then, the longer the chains, the higher the threshold F_v needed to break the monolayer during scanning is.[21] Van der Waals interactions can also be modified by varying the Π value, that is, the intermolecular distance, a factor that also affects the monolayer frictional behavior.[26]

The chemistry of the tip−monolayer interface also modifies the friction response, which is much higher for tip−carboxylic acid than for tip−alkyl chain (this effect was seen in a multilayered SA sample, detecting friction differences between even and odd layers[27]). At the same time, the tip−alkyl chain friction response is much lower than for the tip−SiO_2 interface, a fact that was used in a pioneering work to distinguish CdAr covered areas from a SiO_2 substrate.[24]

The aim of the present work was 3-fold: First, we focused on the topography of AA monolayers extracted at different surface pressures to examine the relationship between surface pressure versus area per molecule isotherm and the molecular conformation after the monolayers were transferred to the mica surface, to obtain information about the molecular tilting angle and the sample morphology. Second, the nanomechanical properties of these monolayers were tested by means of force spectroscopy to measure their mechanical resistance and to relate it with the sample Π value so as to assess the different role of van der Waals and electrostatic interactions in the monolayer cohesion. Third, the nanotribology of these samples was studied by means of F_f versus F_v curves to gain insight into the different frictional stages that range from noncontact to total disruption of the monolayer.

Experimental Procedures

LB Film Preparation. Langmuir films were obtained in a NIMA 1232D1D2 LB trough (area of 1200 cm^2). Pure water (Millipore MilliQ grade) was used as the liquid subphase. A solution of AA 3.2 mM in chloroform was spread over the water subphase, and 15 min lapsed before compression to permit evaporation of the chloroform. The compression speed was set to 50 cm^2/min (2.5 cm/min and 5.2 $Å^2$/molecules/min). The LB films were transferred at constant pressure onto freshly cleaved atomically flat mica surfaces (1 cm × 1 cm sheets). The transfer was performed using a NIMA 1232 D1 dipper at several Π values and at a constant temperature of 24 °C. LB films were obtained following a *Z* deposition and at an extraction speed of 10 mm/min. The measured transfer ratios were close to 100%.

AFM Topographic Measurements. Topographic images, force spectroscopy, and LFM measurements were performed in contact mode with a Dimension 3100 microscope attached to a Nanoscope IV controller (Digital Instruments, Santa Barbara, CA). For topographic measurements, Si_3N_4 triangular tips (OMCL TR400PSA, Olympus) with a nominal spring constant of 0.02 N/m were used. Force curves were obtained before and after capturing an image to ensure that the topographic signal was acquired by applying the minimum F_v. The whole system was enclosed in a metallic isolation box placed on a vibration isolation table (TMC). During all experiments, the temperature and humidity were controlled and maintained at 20−22 °C and 40−50% RH.

Force Spectroscopy. Triangular Si_3N_4 tips with a nominal spring constant (k_v) of 0.5 N/m were used (Microlever Probes model MLCT-AUNM, Veeco). The real k_v value was measured individually for each tip using a thermal noise method[28] in a Force Probe1-D MFP microscope (Asylum Research). Force curves were obtained using the force volume routine implemented in the Nanoscope software, which performs a grid of single force curves in a selected area and ensures that each force curve is obtained in a fresh sample spot. The data analysis was performed with AFM Force Volume Data Analysis software.[29] The penetration depth (or sample penetration) during a force curve was calculated as

$$\text{penetration depth} = \Delta Z - \Delta x \tag{1}$$

ΔZ being the piezo displacement and Δx being the cantilever deflection in the contact region. Then

$$\Delta x = \Delta V/S \tag{2}$$

where ΔV is the increment in the photodetector vertical signal as the tip contacts the sample, and *S* is the sensitivity, which is the slope of the contact region of a force curve performed on a rigid sample.

LFM Measurements. The individual lateral constant (k_l) of each probe was calculated using the Ogletree et al. method.[30] Briefly, a silicon oxide grid with very sharp ridges (Mikro-Masch TGG01) and a known geometry was scanned by the tip while the lateral deflection in the trace and retrace scans was recorded. As the two sides of the ridge were made from the same material, the friction difference between the trace and the retrace scans was directly related to the ridge slopes and cantilever k_l value.

F_f versus F_v curves were obtained as follows: An ascending saw tooth signal from an external function generator (Agilent) was subtracted from the vertical photodetector signal obtained through the Signal Access Module (Digital Instruments) using a homemade electronic card. Then, the resulting voltage was injected into the vertical photodetector signal through the Signal Access Module, allowing the feedback loop on the vertical deflection to maintain a steadily increasing F_v value over the course of the F_f versus F_v experiment. The scan area was set to 300 nm × 300 nm at 6.1 Hz with a 512 pixel × 512 pixel resolution. As a result, an entire F_f versus F_v curve ranging from low to high F_v values was obtained every 84 s. Further experimental details can be found elsewhere.[31] The whole data

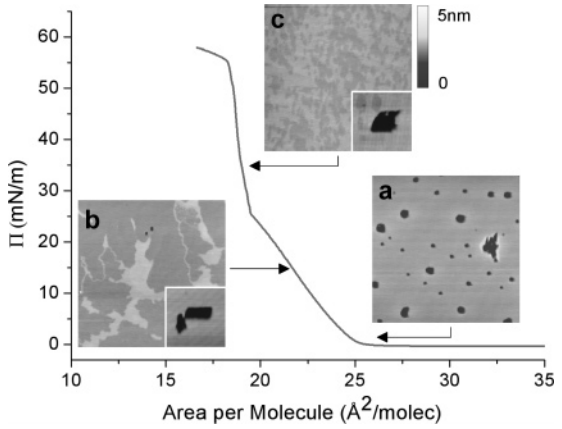

Figure 1. AA Π vs area per molecule isotherm (24 °C). 5 μm × 5 μm AFM contact mode images of AA monolayers extracted at Π values of (a) 1 mN/m, (b) 15 mN/m, and (c) 35 mN/m and supported on mica. The holes observed in panel a show the mica surface. The insets shown in panels b and c correspond to holes created by the AFM tip to expose the mica surface and to measure the AA monolayer thickness.

treatment was performed using Matlab scripts provided by Carpick et al.[32]

Results and Discussion

Monolayer Morphology and Alkyl Chain Orientation versus Π Value. Figure 1 shows the AA monolayer isotherm and the contact AFM images corresponding to monolayers extracted at pressures of (a) 1 mN/m, (b) 15 mN/m, and (c) 35 mN/m. It is clear that the morphology of the monolayers depends on the Π value: At 1 mN/m, the AA molecules form a homogeneous monolayer with the presence of holes, which indicates that the surface is not totally covered. At 15 and 35 mN/m, the mica surface is completely coated by the monolayer, and the presence of different thickness domains is detected, as is plotted in Figure 2a. To perform the monolayer thickness measurements, the bearing option of the Nanoscope software was applied on sample areas that contained a hole showing the mica surface and the studied domain, plotting the height of each pixel with respect to the lowest one and obtaining a height histogram of the selected region. In the samples where the substrate was fully covered, that is, 15 and 35 mN/m, a 1 μm × 1 μm area was scratched to expose the mica surface (insets in Figure 1). The gray dots in Figure 2a correspond to the analysis of individual images captured on different regions of three different samples to ensure reproducibility, and the white dots correspond to the mean sample height values. Interestingly, the monolayer thickness values correspond to discrete values for the three Π values studied in this work: At 1 mN/m, the monolayer thickness is 17.5 ± 0.4 Å; at 15 mN/m, 17.4 ± 0.4 and 22.4 ± 0.2 Å (24.8 ± 0.2 Å domains were sporadically observed); and at 35 mN/m, 22.4 ± 0.2 and 25.0 ± 0.1 Å. These experimental measurements lead to two conclusions: First, the domain thickness tends to be higher as the surface pressure increases, and second, monolayers extracted at different surface pressures share domains with the same thickness. The first conclusion can be correlated to the compression isotherm shown in Figure 1; at 1 mN/m, AA molecules are in the region of low Π values of the liquid condensed phase, and AFM images reveal that molecules aggregate and coalesce, forming a continuous monolayer with an average area per molecule of 25 Å^2. Considering that the molecules arrange in a hexagonal lattice[14] and that the final area per molecule measured during the compression process remains the same once the monolayer has been transferred to the mica substrate, the calculated distance between hydrocarbon chains at 1 mN/m is 5.5 Å, which exceeds the 4.0 Å[33] that corresponds to the minimum distance between -CH_2 groups in adjacent molecules.[34] This higher value of area per molecule leads to a molecular tilting that was studied in the past by means of NEXAFS,[35,36] Raman spectroscopy,[37,38] and FTIR-ATR[39] for a wide variety of fatty acids. Nevertheless, there is a certain discrepancy between the reported tilting angles, mostly attributed to variations in temperature, substrate, or extraction conditions used by the different authors. As the pressure increases (15 mN/m), the mean area per molecule reduces up to 22 Å^2, and the average intermolecular distance is 5.0 Å, while at a pressure of 35 mN/m and with the AA monolayer formally in the solid phase, the area per molecule reduces to 19 Å^2, and the intermolecular distance to 4.7 Å. It should be taken into account that these values are mean measurements and that in the case of the samples extracted at 15 and 35 mN/m, the area per molecule or the intermolecular distance of any of the observed domains are not represented but a macroscopic measurement obtained from the isotherm is.

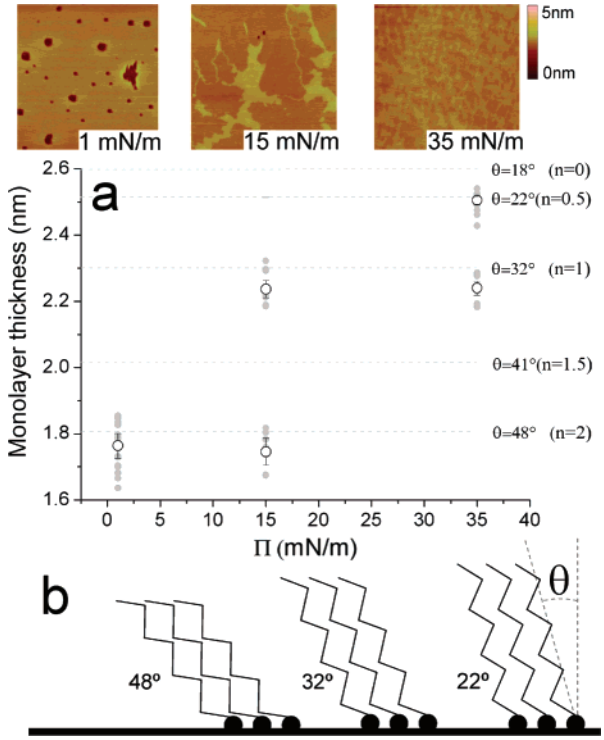

Figure 2. (a) AA monolayer thickness vs Π value. Gray dots indicate individual measurements, and white dots correspond to the mean values. Error bars are calculated as $2s/\sqrt{N}$, s being the standard deviation and N the number of individual measurements obtained for each phase and Π value ($15 < N < 20$). Dotted lines mark the monolayer thickness values and tilting angles (θ) predicted by Barrena et al.,[44] where n is the tilting step in the next-neighbor AA molecule direction. (b) Schematics of the three tilting angles detected in the studied samples.

To quantify the observed molecular tilting angles, we considered an AA molecular length of 27.0 ± 0.1 Å.[16,40] Interestingly, domains showing this thickness value were sporadically seen in our samples near mica defects, which presumably act as nucleation points where the monolayer surface pressure builds up. Now, relating the experimental monolayer thickness values with the AA molecular length, tilting angles of 50° at 1 mN/m, 51 and 34° at 15 mN/m, and 34 and 22° at 35 mN/m were obtained. The significance of discrete molecular tilting angles on monolayers was explored by a pioneering work from Outka et al.,[41] who suggested that the cadmium and

calcium arachidate film thickness and molecular orientation are determined by the interlocking of the monolayer hydrocarbon chains at certain angles that maximize van der Waals interactions, proposing a simple geometrical model to predict the possible orientations. This model was verified for alkylsilanes on mica, where molecules were tilted in a discrete way as pressure was applied by an AFM tip. Alkylthiols on gold were also observed to tilt,[42] and the authors proposed a similar model, which was later improved to account for tilting angles in two dimensions.[43,44] This 2-D model was applied in the present study to explain the experimental AA tilting angles. To do that, it was considered that the intermolecular distance at any tilting angle was constant and equal to the minimum distance between two alkyl chains (4.0 Å). This assumption is more plausible in LB films and alkylsilanes than in alkylthiols because they are not chemically attached to the substrate, so individual molecules can rearrange and modify their molecular area to some extent to maximize the interaction between the alkyl chains. In the case of alkylthiols on gold, and to maintain a constant distance between alkyl chains, the distance between the thiol groups must change, which is not evident because of the covalent bond between the thiols and the gold surface.

The tilting angles predicted by the 2-D model are depicted in Figure 2a as horizontal straight dotted lines.[45] The excellent fitting between the experimental data and the predicted tilting angles suggests that AA alkyl chains are highly oriented and that this orientation is strongly controlled by van der Waals interactions as schematically drawn in Figure 2b. It was found that a coexistence of different molecular tilting angles occurred in the same sample, a fact that can be explained by the presence of substrate defects that induce local surface pressure value differences. We also observed that sample aging[46] influences the morphology of the samples: The area ratio corresponding to the 34 and 22° domains increased with time both in the 15 mN/m and in the 35 mN/m samples. Consequently, the presence of lower tilting angles is favored with time, meaning that the monolayer continues to rearrange after being deposited. The quantification of the rearrangement process and the factors that influence it will be studied in future work.

Force Spectroscopy Measurements. Force spectroscopy has proven to be a very useful technique to test the mechanical properties of a variety of thin films[47] and biological structures.[48,49] Experimentally, a certain F_v is applied on the sample by an AFM probe, while the Δx value is recorded both in the approach and in the retraction processes, so sample compression and relaxation can be sensed and monitored. One of the figures of merit of force curves is the breakthrough force (F_y), which is the necessary F_v to break the sample structure.[50] Sample breakthrough with an AFM tip has been reported in several papers, mostly concerning soft biological structures as phospholipid bilayers.[51] Interestingly, the F_y value can be regarded as a sample fingerprint because it is highly sensitive to structural changes induced by temperature variations, phase transitions,[52] or ionic strength changes in the medium.[53] For all this, it is clear that breakthrough event detection and F_y value quantification can render important information about the different forces that interplay in the structure of fatty acid films.

So as to test the mechanical properties of AA monolayers and to assess the relationship between the F_y value and both the Π value and the tilting angle, force curves were obtained on samples extracted at Π values of 1, 15, and 35 mN/m. In the samples extracted at 15 mN/m, force curves were obtained on the phase tilted by 34°, while in the samples extracted at 35 mN/m, due to the small size of the different thickness domains

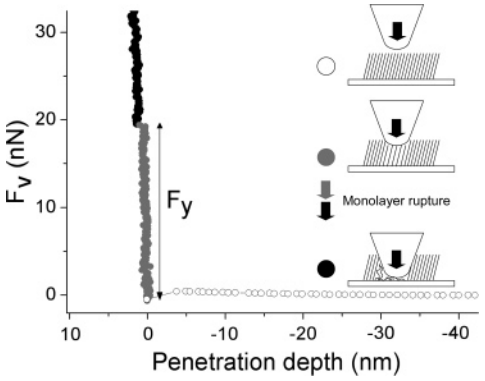

Figure 3. F_v vs penetration depth curve on an AA monolayer extracted at a Π value of 35 mN/m. White dots: noncontact region. Gray dots: elastic monolayer compression and monolayer rupture (F_y). Black dots: hard contact between tip and sample substrate (mica).

(Figure 1c), force curves were obtained both on the phases tilted at 34 and on the phases tilted at 22°. To give an example, a F_v versus sample penetration depth curve obtained on a monolayer extracted at 35 mN/m is shown in Figure 3; initially, the tip and sample are not in contact (white dots). We must emphasize that in this region, eq 1 cannot be applied, so the negative penetration must be understood as the probe approaching the monolayer. Then, as the tip contacts the sample and the F_v value increases (gray region), the cantilever deflects until an abrupt penetration event (sample breakthrough at $F_v = F_y$) takes place around 20 nN. Finally, as the F_v value continues to increase, the tip contacts the mica substrate (black dot region in Figure 3). The total sample penetration, considered as the sample penetration while the tip and the monolayer are in contact, equals the monolayer thickness. Force curves obtained on the different thickness domains observed in samples extracted at 15 mN/m (50 and 34° domains) are distinguished due to the difference in the sample penetration values, but it is not possible to discriminate between the force curves performed on each of the two phases observed in the 35 mN/m sample (34 and 22° domains) because dispersion in the sample penetration values masks the height difference between the two phases.

Figure 4 shows the F_y values for AA monolayers extracted at different surface pressures. Each histogram contains measurements performed with two individually calibrated tips on five different surface spots each, giving F_y values of 13.07 ± 3.24, 15.34 ± 4.94, and 22.94 ± 5.49 nN for 1 mN/m, 15 mN/m (force curves performed on the 34° domains), and 35 mN/m samples, respectively. Then, it is clear that the monolayer resistance to be punctured increases with the monolayer thickness, that is to say, as the molecular tilting decreases. Interestingly, the F_y value is also highly dependent on the AA monolayer phase; while samples extracted at surface pressures of 1 and 15 mN/m are in the liquid condensed phase (F_y values are very similar for the two Π values), the sample extracted at 35 mN/m is in the solid phase (significantly higher F_y value). Because of the high sensitivity of the F_y value to monolayer structural changes, the differences between intermolecular interactions when changing the Π value and the monolayer phase can be correlated with the experimental force spectroscopy results. As was proposed by Israelachvili,[34] the total van der Waals interaction between neighboring alkyl chains equals the energy between adjacent -CH_2 groups, which is 6.9 kJ/mol for an intermolecular distance of 4.0 Å, multiplied by the number of -CH_2 groups per molecule that interact favorably, which is 19 in the case of the AA molecules. This model leads to a maximum interaction when the tilting angle is 0°, while the

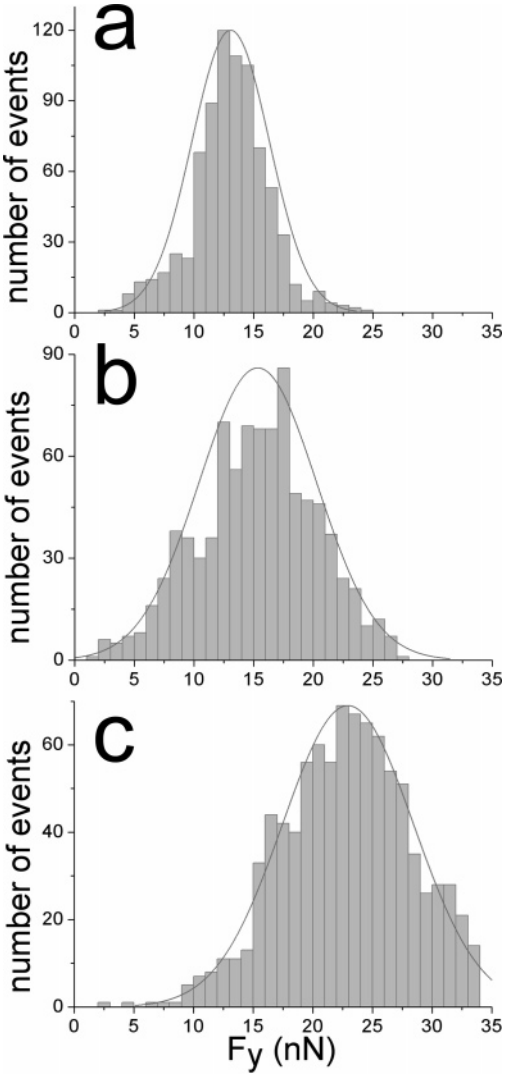

Figure 4. AA monolayer breakthrough force (F_y) histograms for samples extracted at different Π values. (a) 1 mN/m, (b) 15 mN/m, and (c) 35 mN/m where $400 < N < 600$, N being the number of individual F_y measurements at each Π value. Gaussian fitting values: (a) 13.07 ± 3.24 nN, (b) 15.34 ± 4.94 nN, and (c) 22.94 ± 5.49 nN, where the error stands for the standard deviation.

number of favorable -CH_2 interactions is reduced by 1 as the alkyl chains slip 1 notch to accommodate to the next possible tilting angle.[42] According to this, calculated van der Waals energies for samples tilted 22, 34, and 50° are 127.7, 124.2, and 117.3 kJ/mol, respectively,[54] which represents that at 34 and 50°, the van der Waals interaction is 97 and 92% of the interaction at 22°, respectively. The experimental total energy exerted by the tip on the monolayer (E_e) during the breakthrough process can be calculated as

$$E_e = F_y \times \text{penetration depth} \quad (3)$$

If E_e values are normalized the same way, the E_e value needed to break the monolayer at 34 and 50° is 64 and 47% of the E_e value at 22°.[55] Consequently, it is clear that the ΔF_y value as the tilting angle reduces cannot be explained only as a function of the van der Waals interactions between the alkyl chains, so other cohesive forces that also depend on the Π value have to be considered. Indeed, the role of the hydrophilic headgroups in the stability of the monolayers was studied in the past. The presence of hydrogen bonds was detected both between amides[56] and between carboxylic acid groups in multilayers, resulting in a transition temperature increase.[57] The interaction between the polar headgroups and the substrate surface is also important and influences the thermal stability of the monolayers.[58,59] In the present study, the monolayer subphase during compression and extraction is MilliQ water, so, having in mind that the AA pK_a is 7.1, the carboxylic acid groups will be partially deprotonated, interacting electrostatically with both the charged mica surface[60] and the surrounding carboxylic groups. The energetic study of protonated and deprotonated fatty acid monolayers performed by Tippmann-Krayer and Mohwald[61] reported thermal desorption energies of 185 and 76 kJ/mol for magnesium arachidate and AA, respectively, highlighting the significance of electrostatic charges in the structure of the monolayers. Moreover, the monolayer tilting angle was observed to change when switching from SA monolayers to cadmium stearate due to electrostatic interactions,[62] a fact that was also observed by Outka et al.[41] for cadmium and calcium arachidate monolayers. In conclusion, the electrostatic interactions between the partially deprotonated carboxyl groups, between these groups and the charged mica substrate, and the hydrogen bonds between carboxylic acids strongly contribute to the mechanical resistance of AA monolayers.

The dispersion of F_y values for a certain Π value is an important parameter because it is closely related with the fluidity and homogeneity of the monolayer. Previous studies performed in our group concerning the mechanical properties of a variety of phosphatidylcholine bilayers demonstrated that the dispersion of F_y values was always lower when the phospholipid was in a fluid phase than when it was solid.[52] As the sample remains in the fluid phase, the surface is more homogeneous because of the high mobility of the molecules. Then, the monolayer mechanical properties are irrespective of the spot where the force curve is performed, which results in a low dispersion of F_y values. When the sample is cooled down under the transition temperature and becomes solid, packing defects arise in the structure, contributing to a larger dispersion of mechanical properties from spot to spot. Concerning the results presented in Figure 4, the dispersion of F_y values corresponding to the sample extracted at 1 mN/m is the lowest of the three, as this is the sample with weaker intermolecular interactions and a higher area per molecule. This fact leads to a fluidity increase with respect to the other samples, especially the one extracted at 15 mN/m. In the case of the sample extracted at 35 mN/m, the dispersion is promoted by the tight molecular packing but also by the presence of two mixed phases with different structural and mechanical properties.

In conclusion, force spectroscopy measurements have proved to be suitable to assess the mechanical stability of AA monolayers and to relate it with the molecular orientation. Moreover, and to the best of our knowledge, this is the first study that experimentally quantifies the difference in mechanical properties between monolayers that only differ in their molecular tilting angle. Further work will be devoted to studying and isolating the contribution of van der Waals forces, hydrogen bonds and electrostatic interactions in the experimental F_y values to quantify them separately and relate them to the structural resistance of the monolayer.

***F_f* versus *F_v* Measurements.** Figure 5 shows three F_f versus F_v curves performed on AA samples extracted at 1, 15, and 35 mN/m (in the case of the samples extracted at 15 and 35 mN/m, F_f vs F_v curves were obtained for the domains tilted 34 and 22°, respectively). All F_f versus F_v curves were performed from $F_v = 0$ nN up to total monolayer disruption, as can be seen in the topographic images shown in Figure 5, parts 1 and 2.

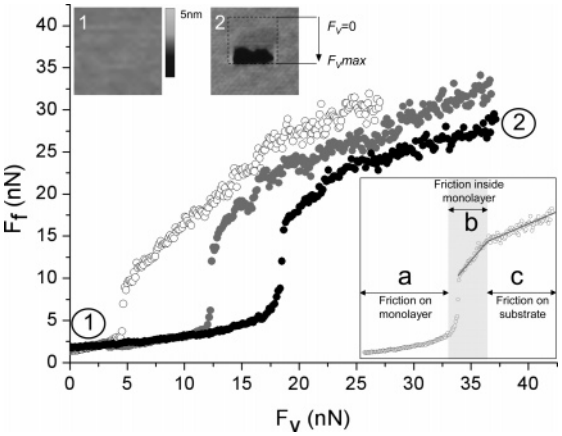

Figure 5. F_f vs F_v curves obtained on AA monolayers extracted at 1 mN/m (white dots), 15 mN/m (gray dots), and 35 mN/m (black dots). Inset: F_f vs F_v curve outline with the three observed friction regimes, going from a soft contact between the tip and the monolayer (a) to film rupture (c). Image 1 (top left): topographic image of the monolayer before obtaining a F_f vs F_v curve. Image 2: after obtaining the F_f vs F_v curve.

Regardless of the Π value, all curves show the same general shape. At low F_v values, there is a linear region corresponding to low F_f values, which ends with an abrupt F_f value increase followed by another linear region with a higher slope than the one observed at low F_v values. Finally, as the F_v value continues to increase, the curve slope decreases, and another linear region appears. These regimes correspond to different tribological processes induced by the increasing F_v applied on the sample and are schematically depicted in the Figure 5 inset. The first regime corresponds to the contact between the tip and the top of the monolayer (Figure 5, inset a). As the Si_3N_4 tip is hydrophilic and the AA alkyl chains are hydrophobic, the resulting F_f signal is extremely low. Besides, the F_f value of ca. 2 nN obtained at $F_v = \sim 0$ nN for all tested Π values can be attributed to adhesive forces promoted by water on the tip apex (experiments performed in air conditions). Very low F_f signals at low F_v values were also observed in behenic acid and stearic acid monolayers and attributed to an elastic deformation regime.[27] These results were supported by molecular dynamics simulations, which predicted that alkyl chains could be compressed by up to 25% of their total length without deforming plastically.[63]

As the F_v value increases, the monolayer cannot withstand its initial structure and deforms plastically (Figure 5, inset b). This effect was reported in the past in alkylsilane monolayers[64] and alkylthiols on gold,[44] where the molecules tilt in discrete steps as a response to the increasing pressure. According to this, we proposed the model depicted in Figure 6 to explain the behavior of the AA monolayers under compression. As a certain F_v value is applied to the sample during scanning, the tip plastically deforms the monolayer (Figure 6b) and slides not on the monolayer but in the monolayer, tilting the molecules as it moves and increasing the contact area between the tip and the surrounding molecules. This fact, besides the extra resistance offered by the molecules that are in front of the tip in an upright conformation, leads to the measured F_f value increase. The topography of the monolayer after obtaining a F_f versus F_v curve (Figure 6) reveals the plastic deformation induced in the monolayer. Interestingly, the molecules do not recover their initial conformation after the F_v is released (Figure 6b), so they possibly attain a stable conformation that maximizes the chains interlocking. Unfortunately, as the k_v value of the tips used for friction measurements is too high, no reliable height measurements could be performed to calculate the molecular tilting in this plastic deformation regime. Once the tip has deformed the monolayer, the F_f value increases linearly until a certain F_v is reached and the monolayer is thoroughly punctured and removed from the surface. Then, the tip contacts the substrate, resulting in a linear relationship between the experimentally measured F_f and the experimentally measured F_v values.

To extract quantitative information from the F_f versus F_v curves, experiments were performed by using two calibrated cantilevers. At least 20 F_f versus F_v curves were recorded for each probe, and two individual samples were tested for each Π value. The chosen figures of merit to quantify the curves were the ΔF_v value while the tip is in contact with the top of the monolayer (ΔF_{vTM}), which corresponds to the region shown in Figure 5, inset a, the slope of this region (μ_{TM}), and the slope of the F_f versus F_v curves when the monolayer is broken and the tip contacts the substrate (Figure 5, inset c) (μ_S). These measurements are shown in Figure 7, where gray dots correspond to individual measurements, and white dots are the calculated mean values. Concerning ΔF_{vTM} (Figure 7a), it is clear that its value increases with the Π value. This means that the F_v needed to break the monolayer increases as the area per molecule and the tilting angle decrease. Then, it was experimentally proven that the F_f versus F_v curves are sensitive to the monolayer molecular packing and are able to discern between the different arrangements that AA molecules undergo depending on the Π value. In fact, these measurements corroborate the force spectroscopy data presented in Figure 4, where the F_y value is a measurement of the mechanical strength of the monolayer. Nevertheless, the different nature of the two mechanical tests should be considered; on one hand, force spectroscopy measurements consist of the exertion of a certain F_v in a single spot, affecting a small number of molecules. On the other hand, LFM measurements affect a larger number of molecules while the tip scans the sample surface. Then, it is clear that the relationship between F_y and ΔF_{vTM} values is not straightforward and is affected by a number of factors such as the tip velocity and scan area. However, it is interesting to note that force spectroscopy and LFM measurements give complementary information about the mechanical resistance of monolayers and are sensitive to different packing densities.

The relationship between F_f and F_v signals is linear for regions a and c in the Figure 5 inset, so μ_{TM} and μ_S can be regarded as the friction coefficients of the monolayer and substrate, respectively. Concerning μ_{TM} values, Figure 7b shows that their magnitude decreases as the Π value increases, ranging from 0.35 to 0.18. This trend can be related to the different compactness of the tested monolayers. At low Π values, the number of structural defects and vacancies is high in the monolayers as shown in Figure 1a, where micrometric holes can be observed. As is well-known, packing defects are prone to increase the F_f value because a defective monolayer provides more pathways to dissipate energy during sliding.[65] As the Π value increases, molecular packing improves, and consequently, both μ_{TM} value and elastic deformation decrease. The measured μ_{TM} values are higher than those expected for a clean Si_3N_4 tip in contact with a surface functionalized with alkyl chains (typically below 0.1[65]), mainly due to AA molecules' transfer from the monolayer to the tip during the LFM experiments.

Dealing with region c in the Figure 5 inset, preliminary experiments performed on clean mica rendered friction coefficients of 0.17 ± 0.03 in air, while μ_S ranged from 0.73 to 0.42. In this case, it is difficult to precisely define the tip−

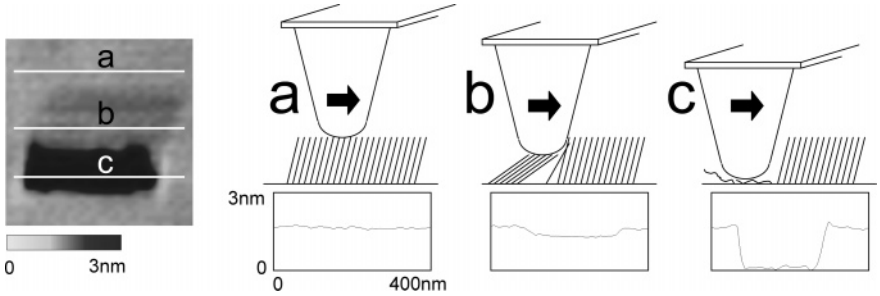

Figure 6. Proposed model for the tip−sample interaction as the F_v value increases during LFM experiments. (a) Elastic sample deformation, no structural changes (low F_f signal). (b) Molecular tilting (plastic deformation) induced by the pressure exerted by the tip, resulting in a F_f value increase. (c) Monolayer rupture and contact with the substrate. These regimes correspond to the a−c regions of the Figure 5 inset. The topographic image was captured after obtaining a F_f vs F_v curve on an AA monolayer extracted at a Π value of 1 mN/m (slow scan axis direction: up−down). The topographic sections under each image are marked as white lines in the topographic image.

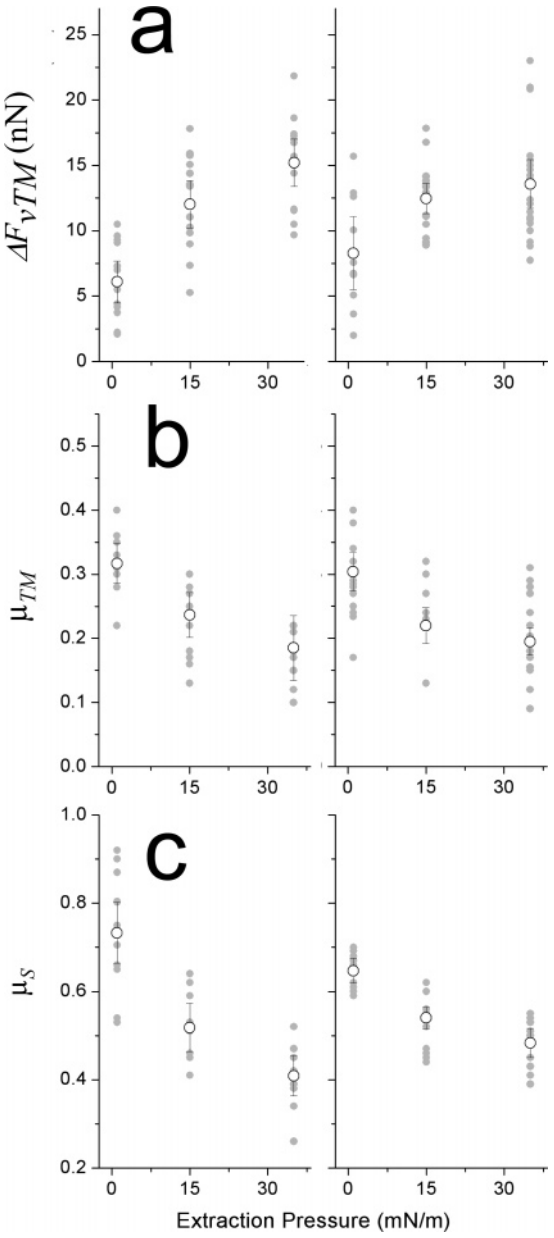

Figure 7. F_f vs F_v curve analysis: (a) ΔF_{vTM} vs Π value, (b) μ_{TM} vs Π value, and (c) μ_S vs Π value. The measurements were obtained for two different samples with two different tips. Gray dots indicate individual measurements, and white dots are the mean values. The error bars are $2s/\sqrt{N}$, N being the number of individual measurements.

sample interface while performing the LFM measurements at high F_v values because the AA monolayer is ruptured and individual molecules are scattered on the substrate surface, increasing the frictional interaction. Interestingly, the μ_S value depends on the Π value, and it decreases when the area per molecule and the tilting angle decrease. We propose that, at low Π values, the weak interactions between molecules let them scatter individually on the area where the monolayer has been removed while performing the LFM experiments, increasing the friction signal between the tip and the sample. However, as the Π value increases, it is more difficult to break the individual interactions between molecules, and we propose that they are expulsed in clusters, leaving a cleaner substrate with frictional properties closer to those of bare mica. According to this, a previous work demonstrated the interplay between the packing density and the molecular expulsion mechanism, concluding that a tight structure leads to a brittle structural collapse, while loose packing is more prone to deform plastically under the exertion of a certain F_v.[13]

Conclusion

The analysis of AFM topographic images of AA monolayers extracted at different Π values reveals that the molecular tilting angle decreases as the monolayer Π value increases. Moreover, the molecular tilting is not a continuous process but takes place in discrete steps, and angles of 50, 50/34, and 34/22° are observed for samples extracted at Π values of 1, 15, and 35 mN/m, respectively, being in excellent accordance with the 2-D chain interlocking model.

Force spectroscopy measurements show that the F_y value strongly depends on the monolayer phase, as experimentally measured in the Π versus area per molecule isotherm (solid phase at 35 mN/m breaks at 22.94 ± 5.49 nN, while the liquid condensed phase monolayer extracted at 15 mN/m breaks at 15.34 ± 4.94 nN), but also on the molecular tilting angle. Consequently, the F_y value can be considered as a fingerprint of the structural conformation of monolayers due to its sensitivity to different molecular orientations. Moreover, due to the fully quantitative nature of the obtained F_y values, they can be used to assess the different interactions involved in the monolayer cohesion. In this particular case, the increment in the F_y value as the Π value increases cannot be explained only as a function of the increasing van der Waals interactions between chains due to the tilting angle reduction. According to this, the electrostatic and H-bond interactions between the carboxylic acid headgroups play an important role in the monolayer mechanical resistance. Further work should be devoted to study the effect of different headgroups, pH conditions, and subphase ions in the experimental F_y value, so as to assess the contribution of these factors to the nanomechanical properties of fatty acid monolayers.

LFM experiments show that the tribological properties of these monolayers highly depend on the applied F_v value, observing three different friction regimes. These regimes correspond to the tip sliding on top of the alkyl chains, the tip plastically deforming the monolayer and inducing molecular tilting, and finally rupturing the monolayer and contacting the substrate. Interestingly, the F_v value that the monolayer can withstand before deforming plastically increases with the Π value, a fact that highlights the sensitivity of LFM to the sample molecular ordering.

Acknowledgment. G.O. thanks Matt Brukman (North Carolina State University) and Robert Carpick (University of Pennsylvania) for providing the Matlab scripts to analyze friction data and Mickey Huson (CSIRO) for the AFM Force Volume Data Analysis software. This work was supported by Generalitat de Catalunya trough Project 2002PIRA 00167 and MCYT through Projects CTQ2004-08046-C02-01 and CTQ2004-08046-C02-02.

References and Notes

(1) Blodgett, K. B. *J. Am. Chem. Soc.* **1935**, *57*, 1007.
(2) Kiessling, V.; Crane, J. M.; Tamm, L. K. *Biophys. J.* **2006**, *91*, 3313.
(3) Tao, A.; Kim, F.; Hess, C.; Goldberger, J.; He, R. R.; Sun, Y. G.; Xia, Y. N.; Yang, P. D. *Nano Lett.* **2003**, *3*, 1229.
(4) Cong, P.; Nanao, H.; Igari, T.; Mori, S. *Appl. Surf. Sci*. **2000**, *167*, 152.
(5) Ren, S. L.; Yang, S. R.; Wang, J. Q.; Liu, W. M.; Zhao, Y. P. *Chem. Mater*. **2004**, *16*, 428.
(6) Leggett, G. J. *Anal. Chim. Acta* **2003**, *479*, 17.
(7) Carpick, R. W.; Salmeron, M. *Chem. Rev.* **1997**, *97*, 1163.
(8) Bhushan, B.; Israelachvili, J. N.; Landman, U. *Nature (London, U.K.)* **1995**, *374*, 607.
(9) Krim, J. *Surf. Sci.* **2002**, *500*, 741.
(10) Gnecco, E.; Bennewitz, R.; Gyalog, T.; Meyer, E. *J. Phys.: Condensed Matter* **2001**, *13*, 619.
(11) Takano, H.; Kenseth, J. R.; Wong, S. S.; O'Brien, J. C.; Porter, M. D. *Chem. Rev.* **1999**, *99*, 2845.
(12) Grant, L. M.; Tiberg, F. *Biophys. J.* **2002**, *82*, 1373.
(13) Oncins, G.; Garcia-Manyes, S.; Sanz, F. *Langmuir* **2005**, *21*, 7373.
(14) Garoff, S.; Deckman, H. W.; Dunsmuir, J. H.; Alvarez, M. S.; Bloch, J. M. *J. Phys.* **1986**, *47*, 701.
(15) Matsumoto, M.; Tanaka, K.; Azumi, R.; Kondo, Y.; Yoshino, N. *Langmuir* **2003**, *19*, 2802.
(16) Mori, O.; Imae, T. *Langmuir* **1995**, *11*, 4779.
(17) Evenson, S. A.; Badyal, J. P. S.; Pearson, C.; Petty, M. C. *J. Phys. Chem.* **1996**, *100*, 11672.
(18) Kajiyama, T.; Oishi, Y.; Hirose, F.; Shuto, K.; Kuri, T. *Langmuir* **1994**, *10*, 1297.
(19) Leuthe, A.; Chi, L. F.; Riegler, H. *Thin Solid Films* **1994**, *243*, 351.
(20) Chunbo, Y.; Desheng, D.; Zuhong, L.; Juzheng, L. *Colloids Surf., A* **1999**, *150*, 1.
(21) Hartig, M.; Chi, L. F.; Liu, X. D.; Fuchs, H. *Thin Solid Films* **1998**, *329*, 262.
(22) Oishi, Y.; Umeda, T.; Kuramori, M.; Suehiro, K. *Langmuir* **2002**, *18*, 945.
(23) Oishi, Y.; Kasagi, T.; Kuramori, M.; Suehiro, K. *Colloids Surf., A* **2000**, *169*, 171.
(24) Meyer, E.; Overney, R.; Brodbeck, D.; Howald, L.; Luthi, R.; Frommer, J.; Guntherodt, H. J. *Phys. Rev. Lett.* **1992**, *69*, 1777.
(25) Kondrashkina, E. A.; Hagedorn, K.; Vollhardt, D.; Schmidbauer, M.; Kohler, R. *Langmuir* **1996**, *12*, 5148.
(26) Oncins, G.; Torrent-Burgues, J.; Sanz, F. *Tribol. Lett.* **2006**, *21*, 175.
(27) Tsukruk, V. V.; Bliznyuk, V. N.; Hazel, J.; Visser, D.; Everson, M. P. *Langmuir* **1996**, *12*, 4840.
(28) Florin, E. L.; Rief, M.; Lehmann, H.; Ludwig, M.; Dornmair, C.; Moy, V. T.; Gaub, H. E. *Biosens. Bioelectron.* **1995**, *10*, 895.
(29) Developed in CSIRO (Australia's Commonwealth Scientific and Industrial Research Organization) by Dr. Mickey Huson, mickey.huson@csiro.au.
(30) Ogletree, D. F.; Carpick, R. W.; Salmeron, M. *Rev. Sci. Instrum.* **1996**, *67*, 3298.
(31) Brukman, M. J.; Marco, G. O.; Dunbar, T. D.; Boardman, L. D.; Carpick, R. W. *Langmuir* **2006**, *22*, 3988.
(32) Scripts are available for non-commercial use at http://mandm.engr.wisc.edu/faculty_pages_carpick/toolbox.htm.
(33) This value is measured perpendicular to the alkyl chains, while the distance measurements extracted from the average area per molecule are measured parallel to the surface.
(34) Israelachvili, J. N. *Intermolecular Surface Forces*, 1st ed.; Academic Press: London, 1985; pp 88−89.
(35) Rabe, J. P.; Swalen, J. D.; Outka, D. A.; Stohr, J. *Thin Solid Films* **1988**, *159*, 275.
(36) Outka, D. A.; Stohr, J.; Rabe, J. P.; Swalen, J. D. *J. Chem. Phys.* **1988**, *88*, 4076.
(37) Rabe, J. P.; Novotny, V.; Swalen, J. D.; Rabolt, J. F. *Thin Solid Films* **1988**, *159*, 359.
(38) Rabe, J. P.; Swalen, J. D.; Rabolt, J. F. *J. Chem. Phys.* **1987**, *86*, 1601.
(39) Ahn, D. J.; Franses, E. I. *J. Phys. Chem.* **1992**, *96*, 9952.
(40) Robinson, I.; Jarvis, D. J.; Sambles, J. R. *J. Phys. D: Appl. Phys.* **1991**, *24*, 347.
(41) Outka, D. A.; Stohr, J.; Rabe, J. P.; Swalen, J. D.; Rotermund, H. H. *Phys. Rev. Lett.* **1987**, *59*, 1321.
(42) Ulman, A.; Eilers, J. E.; Tillman, N. *Langmuir* **1989**, *5*, 1147.
(43) Wurger, A. *Phys. Rev. Lett.* **1999**, *83*, 1696.
(44) Barrena, E.; Ocal, C.; Salmeron, M. *J. Chem. Phys.* **2000**, *113*, 2413.
(45) Depicted tilting angles correspond to $m = 1$ and $n = 0$ (18°), $n = 1/2$ (22°), $n = 1$ (32°), $n = 3/2$ (41°), and $n = 2$ (48°). For a further description of the method, see ref 44.
(46) Pignataro, B.; Panebianco, S.; Consalvo, C.; Licciardello, A. *Surf. Interface Anal.* **1999**, *27*, 396.
(47) Domke, J.; Radmacher, M. *Langmuir* **1998**, *14*, 3320.
(48) Schneider, J.; Barger, W.; Lee, G. U. *Langmuir* **2003**, *19*, 1899.
(49) Kunneke, S.; Kruger, D.; Janshoff, A. *Biophys. J.* **2004**, *86*, 1545.
(50) Loi, S.; Sun, G.; Franz, V.; Butt, H. J. *Phys. Rev. E: Stat., Nonlinear, Soft Matter Phys.* **2002**, *66*.
(51) Franz, V.; Loi, S.; Muller, H.; Bamberg, E.; Butt, H. H. *Colloids Surf., B* **2002**, *23*, 191.
(52) Garcia-Manyes, S.; Oncins, G.; Sanz, F. *Biophys. J.* **2005**, *89*, 4261.
(53) Garcia-Manyes, S.; Oncins, G.; Sanz, F. *Biophys. J.* **2005**, *89*, 1812.
(54) Angles of 32 and 48° correspond to slips of 1 and 2 notches respectively. For 22°, it was considered a 1/2 notch slippage, the possibility experimentally confirmed in ref 43, resulting in a van der Waals interaction loss of 3.45 kJ/mol.
(55) Molecular area obtained during the Langmuir−Blodgett transfer (27, 22, and 19 Å^2 for 1, 15, and 35 mN/m samples) was included in the calculation so as to normalize F_y and E_e to the same number of affected AA molecules.
(56) Du, X. Z.; Shi, B.; Liang, Y. Q. *Langmuir* **1998**, *14*, 3631.
(57) Du, X. Z.; Liang, Y. Q. *J. Chem. Phys.* **2004**, *120*, 379.
(58) Umemura, J.; Takeda, S.; Hasegawa, T.; Takenaka, T. *J. Mol. Struct.* **1993**, *297*, 57.
(59) Ren, Y. Z.; Asanuma, M.; Iimura, K.; Kato, T. *J. Chem. Phys.* **2001**, *114*, 923.
(60) Butt, H. J. *Biophys. J.* **1991**, *60*, 777.
(61) Tippmann-Krayer, P.; Mohwald, H. *J. Phys. Chem.* **1992**, *96*, 5220.
(62) Wang, Y. C.; Du, X. Z.; Guo, L.; Liu, H. J. *J. Chem. Phys.* **2006**, *124*.
(63) Glosli, J. N.; Mcclelland, G. M. *Phys. Rev. Lett.* **1993**, *70*, 1960.
(64) Barrena, E.; Ocal, C.; Salmeron, M. *J. Chem. Phys.* **1999**, *111*, 9797.
(65) Kim, H. I.; Graupe, M.; Oloba, O.; Koini, T.; Imaduddin, S.; Lee, T. R.; Perry, S. S. *Langmuir* **1999**, *15*, 3179.